Electronic Supplementary Information (ESI)

for

Redox-Triggered Controlled Release Systems Based Bi-Layered Nanocomposite Coating with Synergistic Self-Healing Property

Ting Wang,[a] LingHua Tan,[b] ChenDi Ding,[a] MingDong Wang,[a] JianHua Xu,[a,b] and JiaJun Fu[*,a]

[a] School of Chemical Engineering, Nanjing University of Science and Technology, Nanjing, 210094, China.

[b] School of Materials Science & Engineering, Nanjing Institution of Technology, Nanjing, 211169, China.

[*]Corresponding author. Tel.: +86-025-84315520; Fax: +86-025-84315609

E-Mail address: fujiajun668@gmail.com,

1. Characterization of MSNs

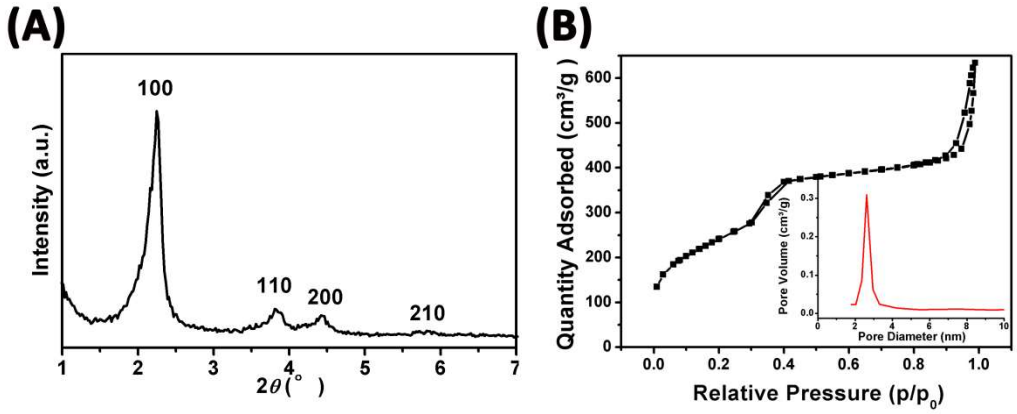

Fig. S1 (A) SA-XRD pattern and (B) N_2 adsorption-desorption isotherm and pore size distribution of MSNs.

2. Synthesis of Compound 1 and Fc-*β*-CD-I

Mono-2-*O*-propargyl-*β*-CD and azidomethylferrocene were synthesized as previously reported in literature[1].

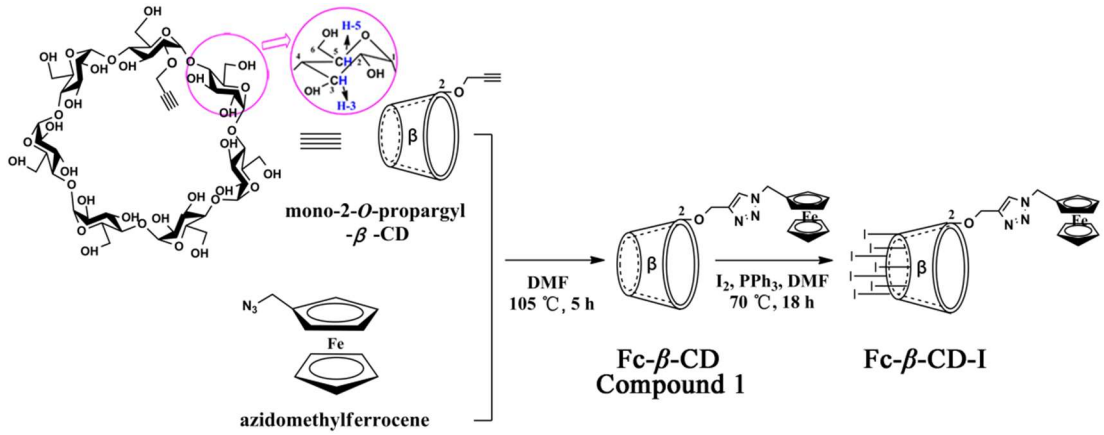

Scheme S1. Synthesis route of Fc-*β*-CD-I.

Compound 1 (mono-2-*O*-[[1-(ferrocenylmethyl)-1*H*-1,2,3-triazol-4-yl]methyl]-*β*-cyclodextrin): A solution of mono-2-*O*-propargyl-*β*-CD (300 mg, 0.256 mmol), Iodo(triethyl phosphite)copper(I) (18mg, 0.05mmol), azidomethylferrocene (68 mg, 0.282 mmol) and anhydrous DMF (10 mL) was stirred under nitrogen atmosphere at 105 ℃ for 5 h. The reaction mixture was poured into acetone (200 mL), and the precipitate was filtered, washed with acetone, and concentrated in vacuo (347 mg, yield 96%).

^{1}H NMR (300 MHz, DMSO-d_6) δ 8.07(s, 1H, H5-C_2HN_3), 5.92(brs, 2H, OH), 5.78 – 5.69(m, 10H, OH), 5.29(d, J = 9.3 Hz, 2H, CHN), 4.87–4.84(m, 8H, H1, CHO), 4.78 (d, J=7.6 Hz, 1H, CHO), 4.63(brs, 1H, OH), 4.52(s, 1H, OH), 4.47–4.43(m, 6H, OH),

4.35(brs, 2H, H_{Cp}), 4.21(s, 5H, $H_{Cp'}$), 4.19(s, 2H, H_{Cp}), 3.85(t, *J*=5.6Hz, 1H, $H3^{A}$), 3.65 – 3.56 (m, 27H, H-3, 5, 6, 6'), 3.43(m, 2H, H-2^{A}, H-4^{A}), 3.41–3.35 (m, H-2, 4, HDO).

^{13}C NMR (75 MHz, DMSO-*d*$_6$) δ 143.65(C4-C_2HN_3), 123.81(C5-C_2HN_3), 102.17 (C-1), 100.26 (C-1^{A}), 82.43(C), 82.21–81.67(C-4), 79.90(C-2^{A}), 73.21–72.26(C-2, C-3, C-5), 72.41(C-3^{A}), 68.79($C_{Cp'}$), 67.71(C_{Cp}), 64.50(CH_2O), 60.08(C-6), 49.25 (CH_2N).

MS (ESI): m/z calcd for $C_{56}H_{83}N_3O_{35}Fe$: 1413.42; found: 1436.41 $[M+Na]^+$.

Fc-*β*-CD-I(mono-2-*O*-[[1-(ferrocenylmethyl)-1*H*-1,2,3-triazol-4-yl]methyl]-heptakis(6-deoxy-6-iodo)-*β*-cyclodextrin): To a solution of Fc-*β*-CD (0.622 g，0.44 mmol) and in anhydrous DMF (9 mL) was added triphenylphosphine (2.308 g, 8.8 mmol), and then the mixture was stirred at 70 ℃ for 18 h under nitrogen atmosphere. After the reaction was cooled to room temperature, a solution of sodium methoxide (0.56 g) in methanol (8 mL) was added dropwise under nitrogen atmosphere and the reaction allowed to stir for 1h. The reaction mixture was poured into methanol (60 mL), and the precipitate was filtered and washed with methanol thoroughly (239 mg, yield 25%).

^{1}H NMR (300 MHz, DMSO-*d*$_6$) δ 8.13(s, 1H, H5-C_2HN_3), 5.95(m, 12H, OH), 5.32 (d, *J* = 15.5 Hz, 2H, CHN), 5.12–4.85 (m, 9H, H1, CHO), 4.53(brs, 2H, H_{Cp}), 4.18(s, 5H, $H_{Cp'}$), 4.15(s, 2H, H_{Cp}), 3.79(t, *J*=9.4Hz, 1H, $H3^{A}$), 3.59(m, 27H, H-3, 5, 6, 6'), 3.36(m, H-2, 4, HDO).

^{13}C NMR (75 MHz, DMSO-*d*$_6$) δ 143.65(C4-C_2HN_3), 128.85(C5-C_2HN_3), 102.09 (C-1), 100.58(C-1^{A}), 83.08(C), 82.82–81.72(C-4), 79.83 (C-2^{A}), 73.48–70.98(C-2, C-3, C-5), 72.08(C-3^{A}), 68.62($C_{Cp'}$), 68.37(C_{Cp}), 64.46(CH_2O), 49.28(CH_2N), 9.32 (C-6).

3. FTIR Spectra

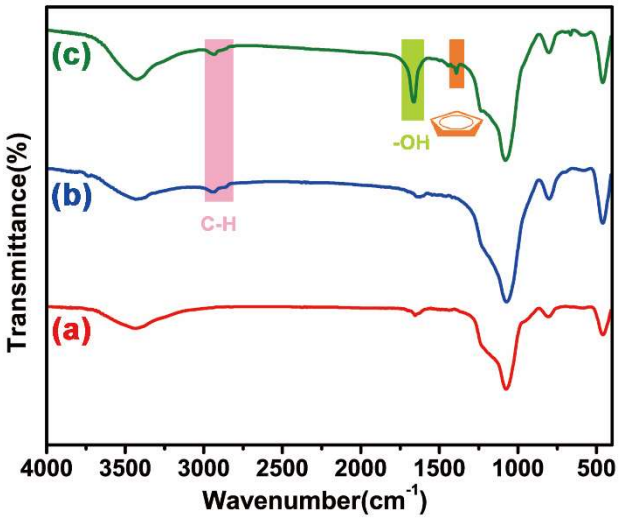

Fig. S2 FTIR spectra of (a) MSNs; (b) MSNs-APTES; and (c) RTSNs 0.

4. Polarization curve of CA

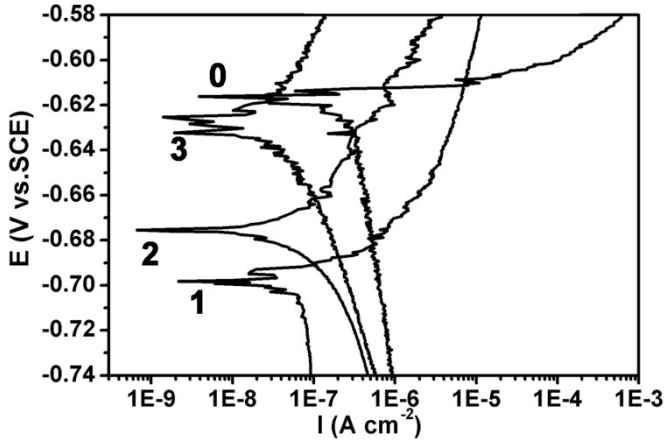

Fig. S3 Polarization curves for AA2024 in 0.5 M NaCl containing different concentrations of CA.

As can be seen in Fig. S3, both the cathodic and anodic reactions were inhibited in 0.5 M NaCl solution with CA, by comparison, the inhibition of the cathodic reactions was more pronounced. Furthermore, the inhibition efficiency (η) increased with the increase of concentrations.

Inhibition efficiency (η) can be calculated from the following equation:

$$\eta = \frac{I_{corr} - I_{corr(inh)}}{I_{corr}} \times 100$$

where I_{corr} and $I_{corr(inh)}$ represent the corrosion current densities without and with the corrosion inhibitor, respectively.

Table S1 Potentiodynamic polarization parameters for the corrosion of AA2024 in 0.5 M NaCl containing different concentrations of CA.

CA conc. ($mg \cdot L^{-1}$)	E_{corr} (mV vs. Ag/AgCl)	I_{corr} ($nA \cdot cm^{-2}$)	η (%)
0	-616.1	238	-
50	-698.3	66.5	72.06
75	-675.4	46	80.67
100	-625.3	39.5	83.40

5. Characterization for the assembly procedure of RTSNs 1

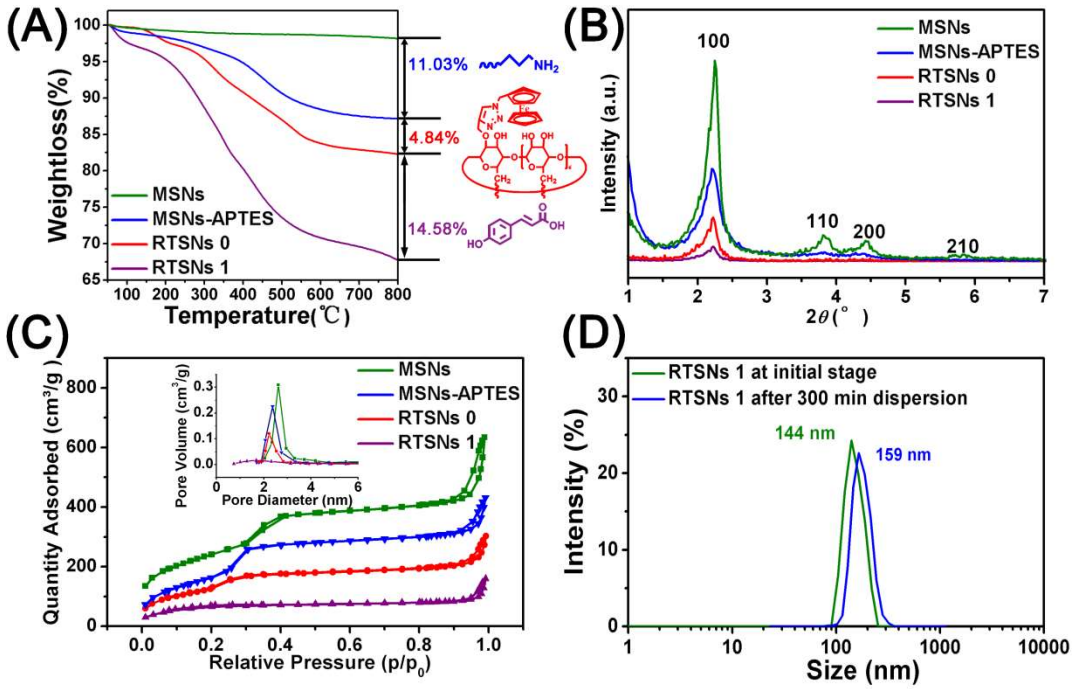

Fig. S4 (A) TGA analyses; (B) SA-XRD pattern; (C) N_2 adsorption-desorption isotherm and pore size distribution of MSNs, MSNs-APTES, RTSNs 0, and RTSNs 1; and (D) the hydrodynamic diameters of RTSNs 1 at initial stage and after 300 min dispersion.

Table S2 Physicochemical properties of the MSNs, MSNs-APTES, RTSNs 0, and RTSNs 1.

Materials	Specific surface area (m^2 g^{-1})	Average pore size (nm)	Pore volume (cm^3 g^{-1})
MSNs	1152.57	2.62	0.98
MSNs-APTES	795.71	2.37	0.67
RTSNs 0	536.77	2.22	0.47
RTSNs 1	170.32	-	0.13

6. Synthesis of Compound 2

Propargyl glycoside was synthesized as previously reported in literature[2].

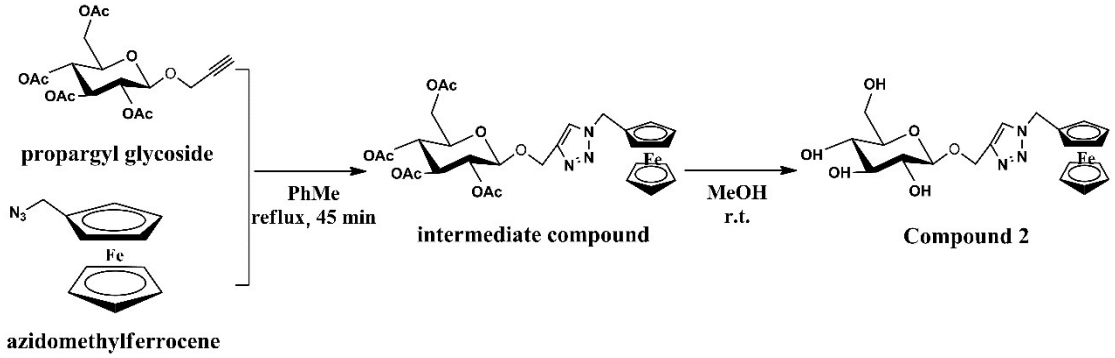

Scheme S2 Synthesis route of Compound 2.

Compound 2: [4-(β-D-Glucopyranosyloxymethyl)-1*H*-1,2,3-triazol-1-yl]methyl ferrocene: Iodo(triethyl phosphite)copper(I) (18mg, 0.05mmol) was added to a solution of azidomethylferrocene (40 mg，0.166 mmol) and propargyl glycoside (71 mg, 0.183mmol) in dry toluene (6 mL). The mixture was stirred under reflux for 45 min. The solvent was removed by evaporation, and the crude product was purified by column chromatography (EtOAc/hexane 2:1) to yield the intermediate compound (100 mg, 95%).

A solution of the intermediate compound (306 mg, 0.488 mmol) in dry MeOH (20 mL) was made alkaline to pH=9.5 with a solution of NaOMe (1 M in methanol) and stirred at room temperature following the reaction by TLC. The solvent was concentrated under vacuum and the crude product was purified by column chromatography (EtOAc/MeOH 3:2) to give pure compound (213 mg, 95%).

^{1}H NMR (300 MHz, D_2O) δ 8.39(s, 1H, H5-C_2HN_3), 5.72(s, 2H, CH_2N)), 5.29(d, *J* = 12.8 Hz, 1H, CHO), 5.23(d, *J* = 12.6 Hz, 1H, CHO), 4.86(d, *J*=8.1 Hz, 1H, H-1), 4.75 (t, *J*=1.3 Hz, 2H, H_{Cp}), 4.66(t, *J*=1.3 Hz, 2H, H_{Cp}), 4.61(brs, 5H, $H_{Cp'}$), 4.21(dd, *J* = 12.5, 1.5 Hz, 1H, H-6), 4.05(dd, *J* = 12.5, 5.3 Hz, 1H, H-6'), 3.82(t, *J*=9.1 Hz, 1H, H-3), 3.74(m, 1H, H-4), 3.70(t, *J* = 1.5 Hz, 1H, H-5), 3.64(t, *J*=8.3 Hz, 1H, H-2).

^{13}C NMR (75 MHz, D_2O): δ 144.1(C4-C_2HN_3), 125.3(C5-C_2HN_3), 101.9(C-1), 82.2 (C_{ipso}), 76.4(C-5), 76.3(C-3), 73.5(C-2), 70.1(C-4), 69.4(C_{Cp},$C_{Cp'}$), 69.2(C_{Cp}), 62.4 (CH_2O), 61.3(C-6), 50.2(CH_2N).

7. Standard calibration curve of Ce (Ⅲ) ions

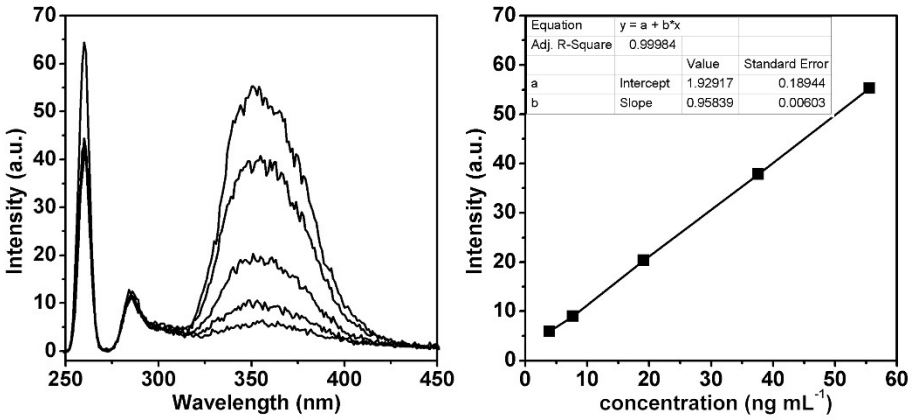

Fig. S5 Standard calibration curve of fluorescence intensity of Cerium(Ⅲ) chloride as a function of the concentration (0-60 ng mL^{-1}).

8. Redox potential-responsive controlled release of CA from RTSNs 1

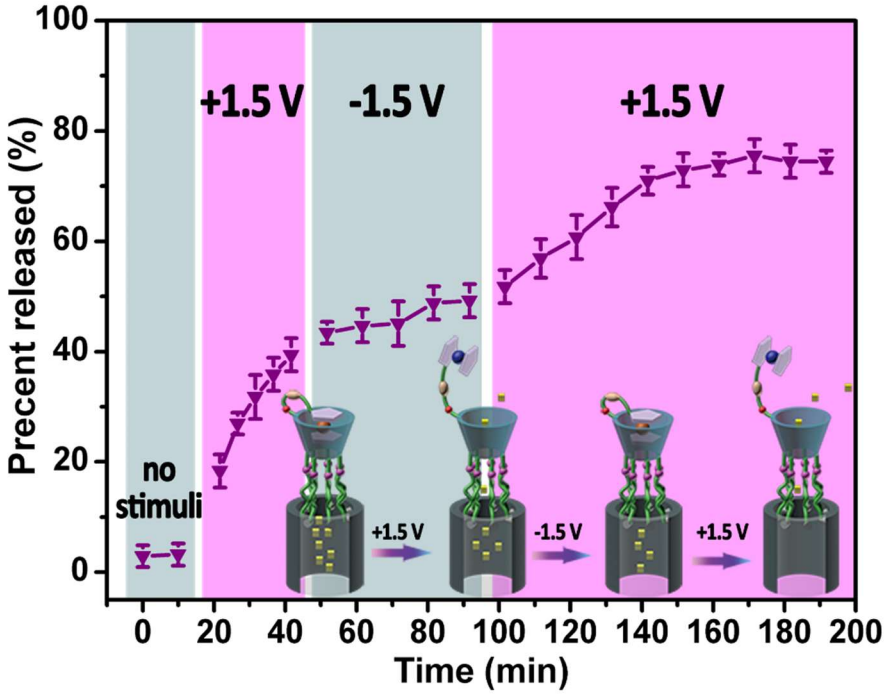

Fig. S6 Redox potential-responsive controlled release of CA from RTSNs 1.

9. pH-stimuli responsive controlled release of RTSNs 1

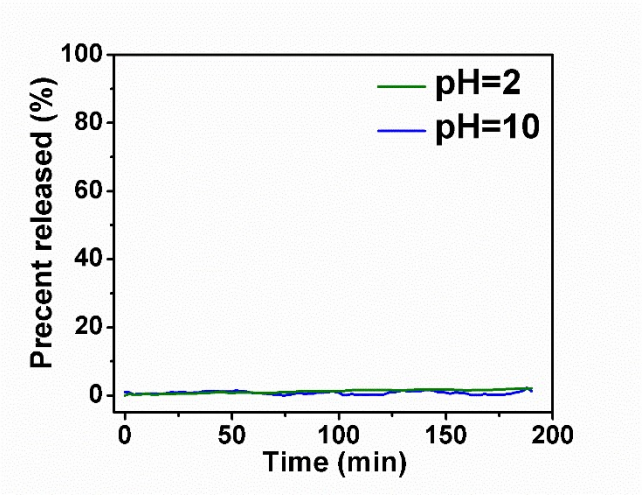

Fig. S7 Release profiles of CA from RTSNs 1 upon pH stimuli.

10. The preparation of Coating(Ⅰ) and Coating(Ⅱ)

Coating(Ⅰ): The preparation procedure of Coating(Ⅰ) was as the same as that of Coating (Ⅲ), expect for the no addition of RTSNs 1 in ZrO_2-SiO_2 sol during the second dip-coating process.

Coating(Ⅱ): The preparation procedure of Coating(Ⅱ) was as the same as that of Coating(Ⅲ), except for the no addition of $Ce(NH_4)_2(NO_3)_6$ in ZrO_2-SiO_2 sol during the first dip-coating process.

11. The influence of introduction of Ce(Ⅳ) and RTSNs 1 on the transparency of the Coating

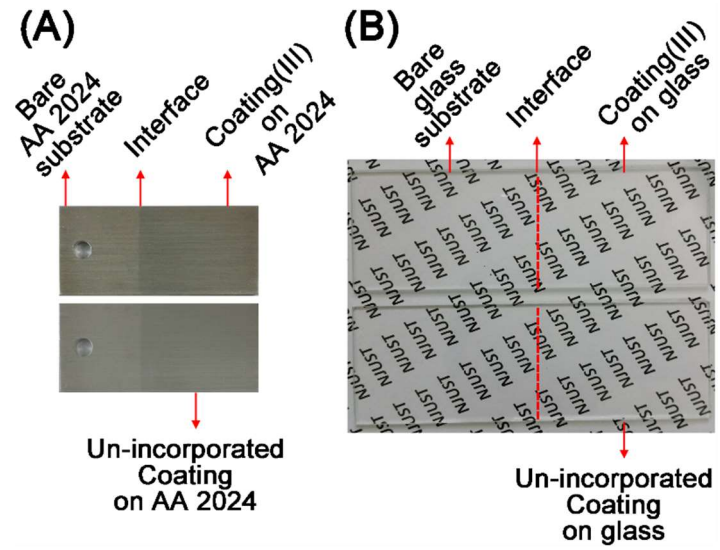

Fig. S8 (A) Optical photographs of the un-incorporated Coating and the bi-layered nanocomposite coating; (B) the glass substrates were coated with the un-incorporated coating and the bi-layered nanocomposite coating.

Fig. S8 shows the surface morphology of the un-incorporated coating and bi-layered nanocomposite coating deposited on both AA2024 and glass. Obviously, the introduction of Ce(Ⅳ) and RTSNs 1 do not change the transparency of the coating.

12. The thermal stability of bi-layered nanocomposite coating

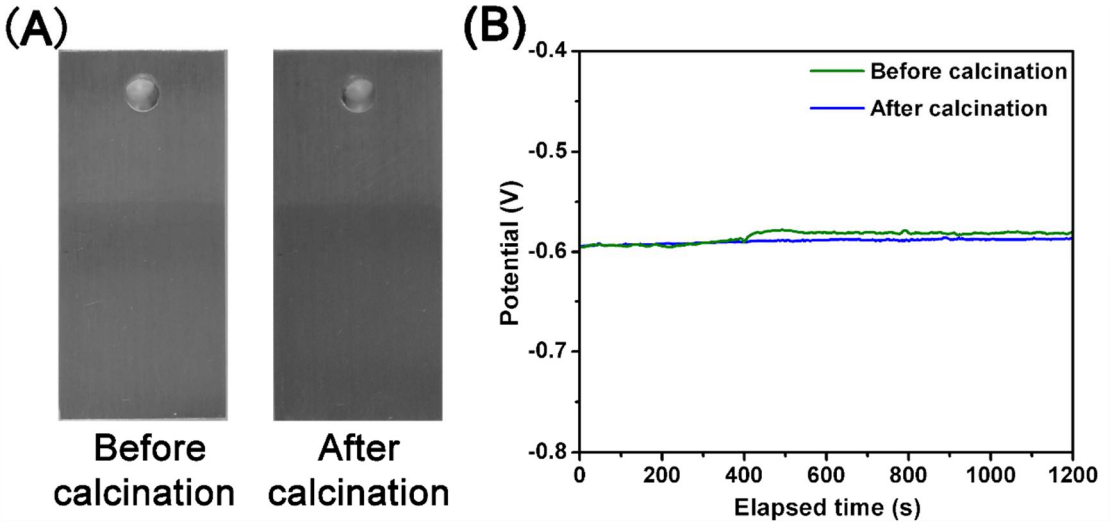

Fig. S9 (A) AA2024 samples coated with the bi-layered nanocomposite coating before and after calcination; (B) the open circuit potential values of the bi-layered nanocomposite coating before and after calcination.

The optical photographs of bi-layered nanocomposite coating before and after calcination are shown in Fig. S9. After calcination at 200℃ for 5 h, the surface morphology of bi-layered nanocomposite coating still remained intact and smooth,

without any cracks. The open circuit potential (OCP) values of bi-layered nanocomposite coating before and after calcination were almost unchanged, indicating the excellent thermal stability.

13.Optical photographs of the three coatings after immersion in NaCl solution

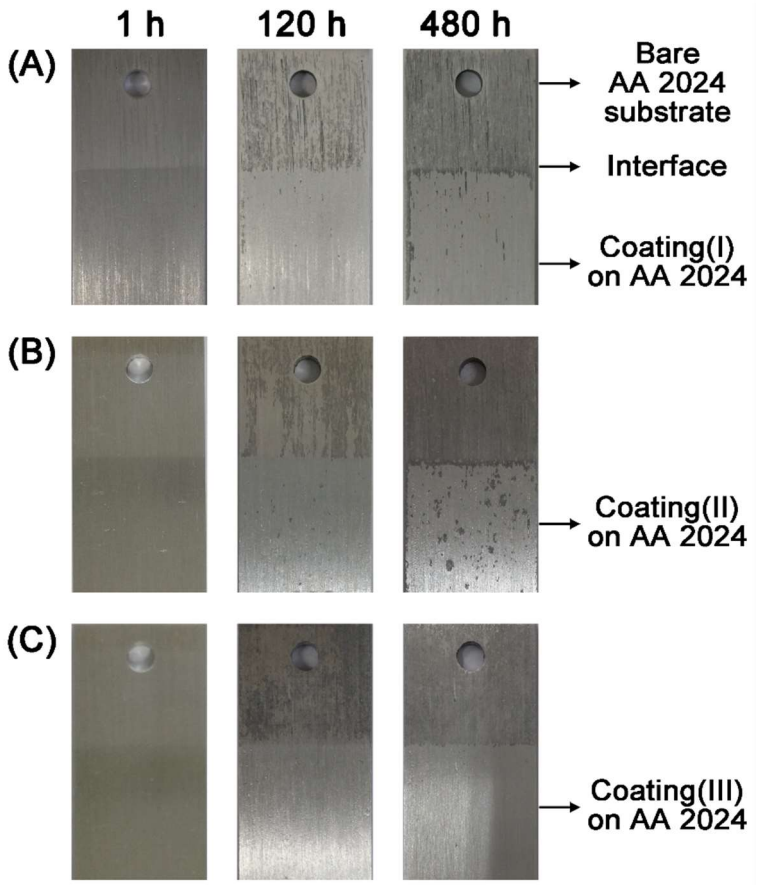

Fig. S10 Optical photographs of Coating(Ⅰ) (A), Coating(Ⅱ) (B) and Coating(Ⅲ) (C) after immersion in 3.5wt% NaCl solution for different stages.

14. The evolution of $|Z|_{0.01Hz}$ of Coating(Ⅰ), Coating(Ⅱ) and Coating(Ⅲ) with artificial scratches.

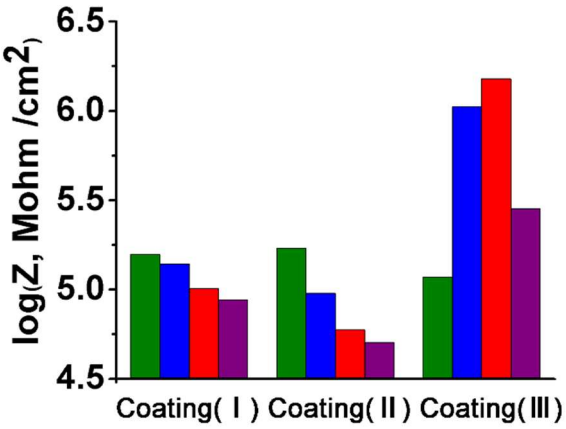

Fig. S11 The evolution of $|Z|_{0.01Hz}$ of Coating(Ⅰ), Coating(Ⅱ) and Coating(Ⅲ) with artificial scratches.

15. Salt Spray Tests

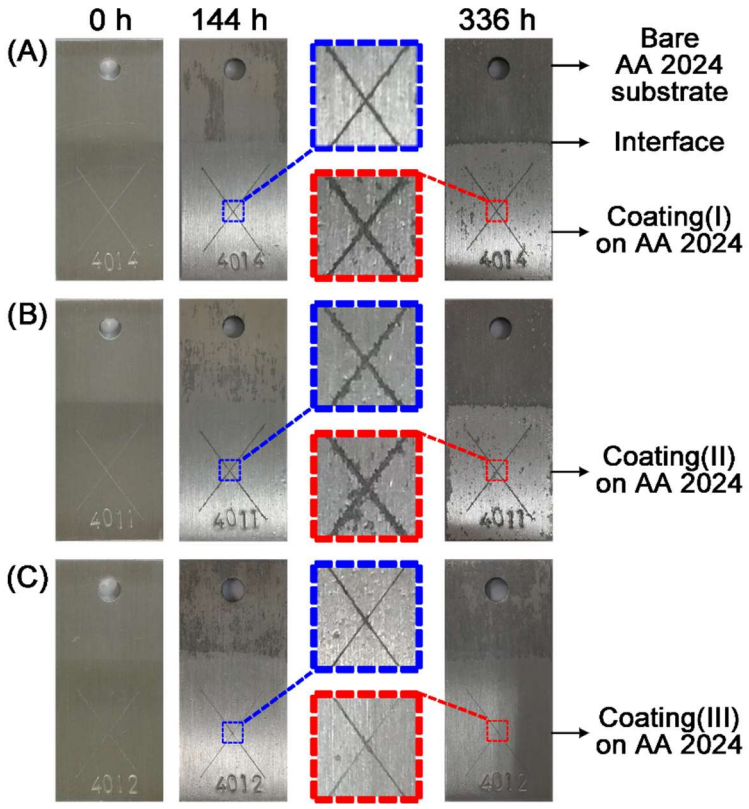

Fig. S12 Optical photographs of Coating(Ⅰ) (A), Coating(Ⅱ) (B) and Coating(Ⅲ) (C) after salt spray tests at different stages.

16. Synergistic inhibition effect of CA and Ce (Ⅲ)

The synergistic inhibition effect of CA and Ce (Ⅲ) on corrosion of AA2024 in 0.5 M NaCl solution was investigated by potentiodynamic polarization methods. The synergistic parameter, η_s, was used to determine whether synergistic inhibition effect is happening, and it is expressed as following equation:

$$\eta_s = \frac{1-\eta_{CA}-\eta_{Ce}+\eta_{CA}\eta_{Ce}}{1-\eta_{CACe}}$$

Where η_{CA} and η_{Ce} are the inhibition efficiencies for CA and Ce(Ⅲ) salts ($CeCl_3 \cdot 7H_2O$), respectively. η_{CACe} is the inhibition efficiency for the mixture of CA and Ce(Ⅲ) salts. In the case η_s=1, CA and Ce(Ⅲ) salts have no synergistic inhibition effect, if η_s > 1, the combination of CA and Ce(Ⅲ) show the synergistic inhibition effect, if η_s < 1, the combination show antagonistic effect.

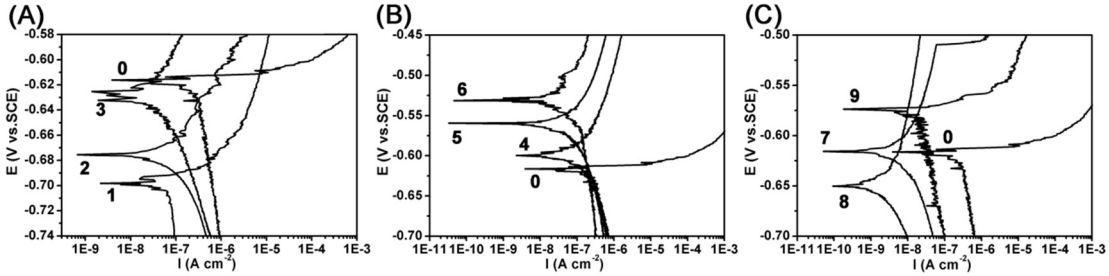

Fig. S13 Tafel polarization curves of AA2024 in 0.5 M NaCl in the various concentration of CA (A), Ce (Ⅲ) salts (B), and CA and Ce (Ⅲ) in the different weight mass ratio (C).

Table S3. Potentiodynamic polarization parameters of AA2024 in 0.5 M NaCl containing different combinations of CA and Ce (Ⅲ) salts.

	CA conc. ($mg \cdot L^{-1}$)	$CeCl_3 \cdot 7H_2O$ conc. ($mg \cdot L^{-1}$)	E_{corr} (mV vs. Ag/AgCl)	I_{corr} ($nA \cdot cm^{-2}$)	η (%)
0	0	0	-616.1	238	-
1	50	0	-698.3	66.5	72.06
2	75	0	-675.4	46	80.67
3	100	0	-625.3	39.5	83.40
4	0	50	-599.7	177	25.63
5	0	75	-559.6	54.8	76.97
6	0	100	-531.4	46.5	80.46
7	50	100	-615.6	3.87	98.63
8	75	75	-650.2	3.10	98.70
9	100	50	-573.8	8.95	96.83

Table S4 The synergistic parameters obtained by combinations of CA and Ce(Ⅲ) salts

CA conc. ($mg \cdot L^{-1}$)	$CeCl_3 \cdot 7H_2O$ conc. ($mg \cdot L^{-1}$)	η_s
50	100	3.99
75	75	3.42
100	50	3.89

As can be seen in Table S4, all the combinations of CA and Ce(Ⅲ) salts show the synergistic inhibition effect, which will ensure that in CA and Ce(Ⅲ) gathered in the scratched area can exhibit the synergistic inhibition effect.

Reference

[1] T. Wang, G. P. Sun, M. D. Wang, B. J. Zhou and J. J. Fu, *ACS Appl. Mater. Interface*, 2015, **7**, 21295-21304.

[2] R. J. Kaufman and R. S. Sidhu, *J. Org. Chem.*, 1982, **47**, 4941-4947.